ISSN 0030-400X, Optics and Spectroscopy, 2014, Vol. 116, No. 3, pp. 348–359. © Pleiades Publishing, Ltd., 2014.

SPECTROSCOPY OF ATOMS AND MOLECULES

Molecular Structure, Vibrational Spectral Investigation and the Confirmation Analysis of 4-Methylesculetin Molecule[1]

Y. Erdogdu[a], *, M. Guzel[b], M. T. Güllüoğlu[a], M. Amalanathan[c], S. Saglam[d], and I. Hubert Joe[c]

[a] *Department of Physics, Ahi Evran University, Kirsehir, 40040 Turkey*

[b] *Department of Computer Programming, Ahi Evran University Mucur Technical Vocational School, Mucur, Kırşehir, 40500 Turkey*

[c] *Centre for Molecular and Biophysical Researches, Department of Physics, Mar Ivanios College, Thiruvananthapuram Kerala, 695015 India*

[d] *Department of Physics, Gazi University, Teknikokullar, Ankara, 06500 Turkey*

**e-mail: yusuferdogdu@mail.com*

Received March 25, 2013

Abstract—In this work, FT-IR, FT-Raman, and FT-NMR spectra of 4-Methylesculetin molecule are presented for the first time. FT-IR, FT-Raman, and FT-NMR spectra of 4MEC have been recorded and analyzed. The FT-IR and FT-Raman spectra of this molecule are recorded at 4000–400 cm^{-1} and 50–3500 cm^{-1}, respectively. The infrared vibrational frequencies, absolute intensities, potential energy profile, HOMO–LUMO plot and NBO analysis of the molecule have been also predicted using Becke's three-parameter hybrid B3LYP method in the density functional theory DFT method. Calculated and experimental data are in good agreement.

DOI: 10.1134/S0030400X14030059

1. INTRODUCTION

The coumarin derivatives are known to have diverse applications as anticoagulants, spasmolytics, anticancer drugs, or as plant growth-regulating agents [1–4]. Their complexation ability in respect to different metal ions has been studied and discussed widely in a considerable number of investigations [5–9]. It has been found that the binding of a metal to the coumarin moiety retains or even enhances its biological activity [10–12]. Various types of coumarin substitutions in their skeletal structure can influence their biological activity. Therefore, a comprehensive structure–system–activity relationship study of coumarins with special respect to carcinogenicity, mutagenicity, and cancer-preventing activity would be of high interest. Recently considerable attention has been focused on biological activity displayed by the coumarins, especially byesculetin [13]. Esculetin and 4-methylesculetin as coumarin derivatives have a diphenolic structure contained in many plants, such as Citrus limonia and Euphorbia lathyris. It has multiple biological activities, including of the inhibition of the xanthine oxidize activity [8], platelet aggregation [14], and the induction apoptosis. In addition, esculetin shows antioxidative activity [15, 16], an inhibitory effect on the growth of human breast cancer [17]. On the other hand the pharmaceuticals and agrochemicals containing catechol skeleton, represent one of the most ubiquitous families of natural antioxidants [18–20].

Modern FT-IR and the near infrared (NIR) FT-Raman spectroscopies have proven to be an exceptionally powerful technique for solving many drug molecules, biological molecules, and the natural products. It has been extensively employed both in the study of chemical kinetics and chemical analysis. Since fluorescence-free Raman spectra and computed results help in the unambiguous identification of vibrational modes and provide deeper insight into the bonding and structural features of complex organic molecular systems [21, 22]. The advent of fast computers along with sophisticated computational methods makes the task of solving various structural chemical problems easily. Density functional theory (DFT) has become an efficient tool in the prediction of molecular structure, conjugation, hydrogen bonding harmonic force field, vibrational frequencies, and IR and Raman activities of the bioactive molecule [23–28]. The present work deals with the FT-IR and FT-Raman spectral investigations of 4-Methylesculetin supported by DFT calculation to understand the structural and bonding features, electron delocalization, and the intramolecular charge transfer interactions. The natural bond orbital (NBO) analysis and the distribution of electric charges on atoms of free molecule of 4-Methylesculetin compounds also were investigated by using the DFT computation.

[1] The article is published in the original.

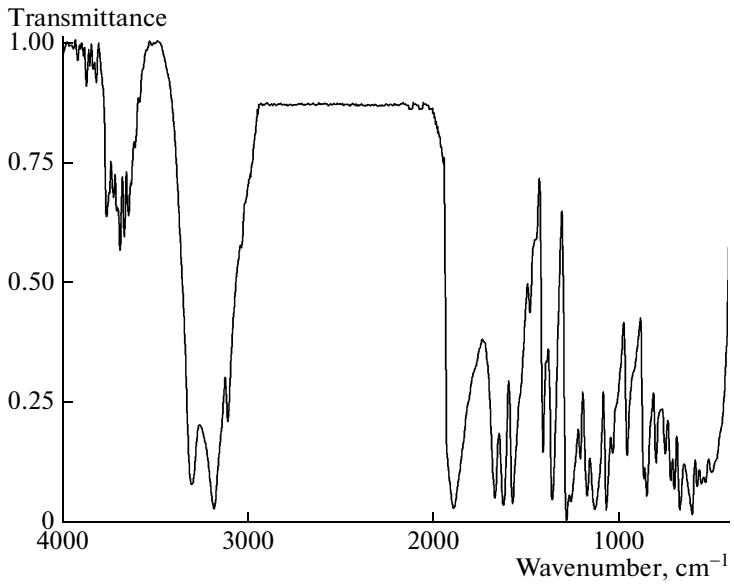

Fig. 1. Experimental FT-IR spectra of 4-methylesculetin molecule.

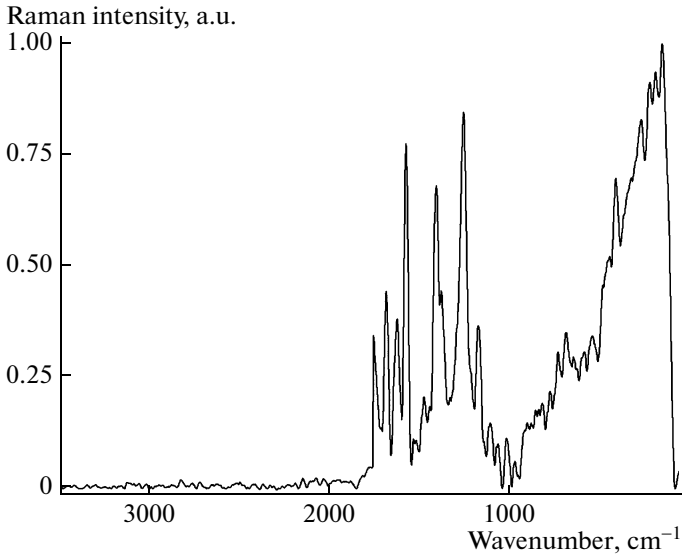

Fig. 2. Experimental FT-Raman spectra of 4-methylesculetin molecule.

2. EXPERIMENTAL

The FT-IR spectrum of this molecule is recorded in the region 4000–400 cm^{-1} on IFS 66V spectrophotometer using KBr pellet technique is shown in Fig. 1. The FT-Raman spectrum of 4MESC has been recorded using 1064 nm line of Nd:YAG laser as excitation wavelength in the region 50–3500 cm^{-1} on Bruker FRA 106/S are shown in Fig. 2. The ^{1}H and ^{13}C NMR spectra are taken in chloroform solutions and all signals are referenced to TMS on a Bruker Superconducting FT-NMR Spectrometer. All NMR spectra are measured at room temperature.

3. COMPUTATIONAL DETAILS

The calculations were performed at DFT levels by using Gaussian 09 [29] program package; invoking gradient geometry optimization [30]. In order to establish the stable possible conformations, the conformational space of title molecule was scanned with molecular mechanic simulations. This calculation was performed with the Spartan 10 program [31]. For meeting the requirements of both accuracy and computing economy, theoretical methods and basis sets should be considered. Density functional theory (DFT) has been proved to be extremely useful in treat-

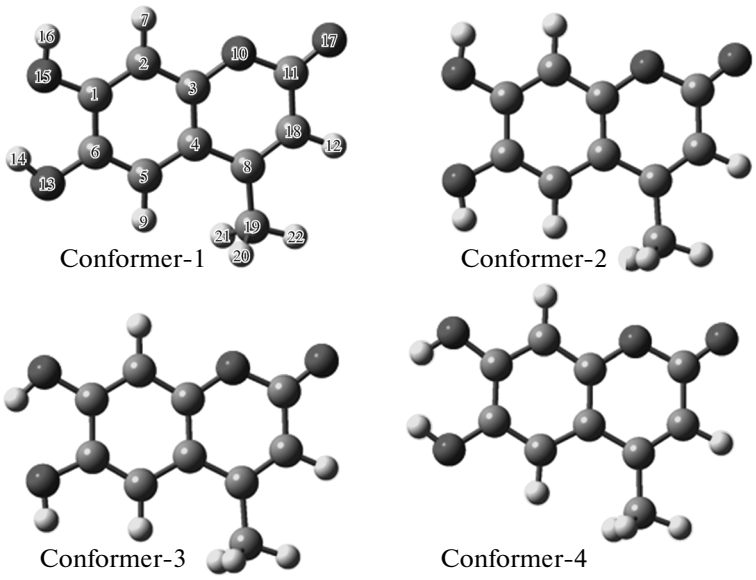

Fig. 3. All conformer and atomic numbering of the 4–metyhylesculetin molecule.

ing electronic structure of molecules. The basis set cc-pVDZ was used for the conformational analysis. The optimized structural parameters were used in the vibrational frequency calculations at the DFT level to characterize all stationary points as minima.

Then, vibrationally averaged nuclear positions of 4MESC were used for harmonic vibrational frequency calculations resulting in IR and Raman frequencies together with intensities and Raman depolarization ratios. In the present work, the DFT method B3LYP with cc-pVDZ, cc-pVTZ and cc-pVQZ basis sets were used for the computation of molecular structure, vibrational frequencies and energies of optimized structures. The vibrational modes were assigned on the basis of TED analysis for higher basis set (B3LYP/cc-pVDZ), using SQM program [32].

It should be noted that Gaussian 03W package is able to calculate the Raman activity. The Raman activities were transformed into Raman intensities using Raint program [33] by the expression:

$$I_i = 10^{-12}(\nu_0 - \nu_i)^4 \frac{1}{\nu_i} RA_i, \quad (1)$$

Table 1. Energetic of the four conformers calculated at the B3LYP/cc-pVDZ level

Conformation	E, Hartree	ΔE, kcal/mol	Dip. Mom., D
1	−686.83073582	0.000	4.345
2	−686.82438414	3.985	4.732
3	−686.83047963	0.160	7.327
4	−686.81897294	7.381	6.438

where I_i is the Raman intensity, RA_i is the Raman scattering activities, ν_i is the wavenumber of the normal modes and ν_0 denotes the wavenumber of the excitation laser [34].

The ^{1}H and ^{13}C NMR chemical shifts calculations of the conformer 1 of the 4MESC molecule were made by using B3LYP functional with cc-pVDZ, cc-pVQZ and cc-pVTZ basis sets. The GIAO (Gauge Including Atomic Orbital) method is one of the most common approaches for calculating isotropic nuclear magnetic shielding tensors [35, 36]. For the same basis set size GIAO method is often more accurate than those calculated with other approaches [37, 38]. The NMR spectra calculations were performed by Gaussian 03 program package. The calculations reported were performed in chloroform solution using IEF–PCM model as well as gas phase in agreement with experimental chemical shifts obtained in chloroform solution.

4. RESULTS AND DISCUSSION

4.1. Molecular Geometry

The numbering scheme for 4MESC is shown in Fig. 3. Optimized bond parameters were calculated by using B3LYP with cc-pVDZ basis set. To find stable conformers, a meticulous conformational analysis was carried out for the title molecule. Rotating each 10 degree intervals around the free rotation bonds, conformational space of the title molecule was scanned by molecular mechanic simulations and then full geometry optimizations of these structures were performed by B3LYP/cc-pVDZ method. Results of geometry optimizations indicated that the title mole-

Table 2. Optimized geometric parameters of 4MESC molecule

Theoretical (B3LYP)				Experimental	Theoretical (B3LYP)				Experimental
Parameters	cc-PVDZ	cc-PVTZ	cc-pVQZ	X-Ray [39]	Parameters	cc-PVDZ	cc-PVTZ	cc-pVQZ	X-Ray [39]
Bond lengths, Å					$C_8–C_{19}–H_{21}$	111.0	111.0	111.0	109.4
$C_1–C_2$	1.388	1.381	1.381	1.373	$C_8–C_{19}–H_{22}$	111.1	110.9	110.9	109.4
$C_1–C_6$	1.415	1.406	1.405	1.398	$H_{20}–C_{19}–H_{21}$	106.8	107.0	107.0	109.4
$C_1–O_{15}$	1.369	1.368	1.366	1.362	$H_{20}–C_{19}–H_{22}$	108.3	108.3	108.3	109.5
$C_2–C_3$	1.400	1.391	1.391	1.383	$H_{21}–C_{19}–H_{22}$	108.3	108.3	108.3	109.4
$C_2–H_7$	1.092	1.082	1.081	0.930	Dihedral angles (deg)				
$C_3–C_4$	1.408	1.400	1.400	1.372	$C_6–C_1–C_2–C_3$	0.0003	0.0008	0.002	2.37
$C_3–O_{18}$	1.363	1.360	1.359	1.382	$C_6–C_1–C_2–H_7$	−179.90	−180.0	−180.0	−177.5
$C_4–C_5$	1.413	1.405	1.405	1.407	$O_{15}–C_1–C_2–C_3$	179.90	180.0	179.9	177.9
$C_4–C_8$	1.454	1.447	1.447	1.445	$O_{15}–C_1–C_2–H_7$	0.0001	0.0004	0.0001	2.18
$C_5–C_6$	1.385	1.377	1.377	1.370	$C_2–C_1–C_6–C_5$	0.0	0.0	0.0	−1.59
$C_5–H_9$	1.089	1.079	1.079	0.930	$C_2–C_1–C_6–O_{13}$	−180.0	−180.0	−179.9	−179.9
$C_6–O_{13}$	1.362	1.362	1.361	1.362	$O_{15}–C_1–C_6–C_5$	179.9	179.9	179.9	178.6
$C_8–C_{10}$	1.361	1.352	1.352	1.354	$O_{15}–C_1–C_6–O_{13}$	0.0002	0.0004	0.0001	0.29
$C_8–C_{19}$	1.503	1.500	1.499	1.490	$C_2–C_1–O_{15}–H_{16}$	0.0	0.0002	0.0	13.18
$C_{10}–C_{11}$	1.455	1.448	1.448	1.415	$C_6–C_1–O_{15}–H_{16}$	−180.0	−180.0	−180.0	−166.86
$C_{10}–H_{12}$	1.090	1.080	1.079	0.930	$C_1–C_2–C_3–C_4$	0.0003	0.0008	0.0002	2.33
$C_{11}–O_{17}$	1.207	1.202	1.201	1.232	$C_1–C_2–C_3–O_{18}$	−179.9	−179.9	−179.9	−178.0
$C_{11}–O_{18}$	1.399	1.392	1.390	1.363	$H_7–C_2–C_3–C_4$	179.9	180.0	180.0	177.6
$O_{13}–H_{14}$	0.971	0.965	0.963	0.820	$H_7–C_2–C_3–O_{18}$	−0.0005	−0.0013	−0.0003	−2.04
$O_{15}–H_{16}$	0.968	0.962	0.960	0.819	$C_2–C_3–C_4–C_5$	0.0	0.0	0.0	1.38
$C_{19}–H_{20}$	1.102	1.092	1.091	0.960	$C_2–C_3–C_4–C_8$	179.9	179.9	179.9	178.9
$C_{19}–H_{21}$	1.102	1.092	1.091	0.960	$O_{18}–C_3–C_4–C_5$	179.9	179.9	179.9	179.0
$C_{19}–H_{22}$	1.098	1.087	1.086	0.960	$O_{18}–C_3–C_4–C_8$	−0.0022	−0.0057	−0.0014	−1.42
Bond angles (deg)					$C_2–C_3–O_{18}–C_{11}$	179.9	180.0	179.9	174.7
$C_2–C_1–C_6$	120.7	120.7	120.7	120.1	$C_4–C_3–O_{18}–C_{11}$	0.0031	0.0077	0.0019	5.57
$C_2–C_1–O_{15}$	124.4	124.0	123.9	122.5	$C_3–C_4–C_5–C_6$	−0.0003	−0.0008	−0.0002	−0.52
$C_6–C_1–O_{15}$	114.7	115.2	115.3	117.3	$C_3–C_4–C_5–H_9$	179.9	180.0	179.9	179.4
$C_1–C_2–C_3$	119.3	119.3	119.2	118.6	$C_8–C_4–C_5–C_6$	179.9	179.9	−179.9	177.92
$C_1–C_2–H_7$	121.6	121.4	121.4	120.6	$C_8–C_4–C_5–H_9$	0.0012	−0.0031	0.0008	2.07
$C_3–C_2–H_7$	118.9	119.1	119.2	120.6	$C_3–C_4–C_8–C_{10}$	−0.0015	−0.0036	−0.0009	−1.05
$C_2–C_3–C_4$	121.1	121.3	121.3	123.2	$C_3–C_4–C_8–C_{19}$	179.9	179.9	179.9	179.44
$C_2–C_3–O_{18}$	116.4	116.5	116.5	114.9	$C_5–C_4–C_8–C_{10}$	180.0	179.9	179.9	176.32
$C_4–C_3–O_{18}$	122.4	122.1	122.0	121.7	$C_5–C_4–C_8–C_{19}$	−0.0008	−0.0019	−0.0005	−3.19
$C_3–C_4–C_5$	118.2	118.1	118.1	116.8	$C_4–C_5–C_6–C_1$	0.0003	0.0008	0.0002	0.65
$C_3–C_4–C_8$	117.7	117.7	117.7	118.0	$C_4–C_5–C_6–O_{13}$	179.9	179.9	180.0	179.0
$C_5–C_4–C_8$	124.0	124.1	124.1	125.0	$H_9–C_5–C_6–C_1$	−179.9	−180.0	−179.9	−179.3
$C_4–C_5–C_6$	121.2	121.2	121.2	121.3	$H_9–C_5–C_6–O_{13}$	−0.0003	−0.0007	−0.0002	−0.93
$C_4–C_5–H_9$	120.9	120.7	120.6	119.3	$C_1–C_6–O_{13}–H_{14}$	−0.0002	−0.0003	−0.0001	−1.35
$C_6–C_5–H_9$	117.8	118.0	118.0	119.3	$C_5–C_6–O_{13}–H_{14}$	180.0	179.9	180.0	179.7
$C_1–C_6–C_5$	119.2	119.3	119.3	119.7	$C_4–C_8–C_{10}–C_{11}$	−0.0043	−0.0114	−0.0028	−0.46
$C_1–C_6–O_{13}$	120.2	120.5	120.6	121.5	$C_4–C_8–C_{10}–H_{12}$	179.9	179.9	179.9	179.4
$C_5–C_6–O_{13}$	120.4	120.1	120.0	118.6	$C_{19}–C_8–C_{10}–C_{11}$	179.9	179.9	179.9	179.0
$C_4–C_8–C_{10}$	118.5	118.7	118.7	118.2	$C_{19}–C_8–C_{10}–H_{12}$	−0.002	−0.0053	−0.0012	−1.03
$C_4–C_8–C_{19}$	120.1	120.1	120.1	120.9	$C_4–C_8–C_{19}–H_{20}$	59.33	59.461	59.475	47.97
$C_{10}–C_8–C_{19}$	121.2	121.0	121.0	120.7	$C_4–C_8–C_{19}–H_{21}$	59.32	59.462	59.474	72.69
$C_8–C_{10}–C_{11}$	123.4	123.3	123.3	123.0	$C_4–C_8–C_{19}–H_{22}$	179.9	179.9	180.0	167.3
$C_8–C_{10}–H_{12}$	121.7	121.6	121.6	118.5	$C_{10}–C_8–C_{19}–H_{20}$	120.6	120.5	120.5	132.1
$C_{11}–C_{10}–H_{12}$	114.8	114.9	115.0	118.4	$C_{10}–C_8–C_{19}–H_{21}$	−120.6	−120.5	−120.5	−107.8
$C_{10}–C_{11}–O_{17}$	126.5	126.5	126.4	123.1	$C_{10}–C_8–C_{19}–H_{22}$	0.0	−0.0014	−0.0005	−12.14
$C_{10}–C_{11}–O_{18}$	115.9	115.8	115.8	117.8	$C_8–C_{10}–C_{11}–O_{17}$	−179.9	179.9	−179.9	−176.8
$O_{17}–C_{11}–O_{18}$	117.4	117.6	117.7	114.4	$C_8–C_{10}–C_{11}–O_{18}$	0.009	0.0237	0.0058	4.36
$C_6–O_{13}–H_{14}$	107.2	108.4	108.7	109.5	$H_{12}–C_{10}–C_{11}–O_{17}$	0.015	0.040	0.0097	3.20
$C_1–O_{15}–H_{16}$	109.9	110.4	110.7	109.5	$H_{12}–C_{10}–C_{11}–O_{18}$	−179.9	−179.9	−179.9	−175.6
$C_3–O_{18}–C_{11}$	121.9	122.1	122.2	121.1	$C_{10}–C_{11}–O_{18}–C_3$	−0.008	−0.0214	−0.0053	−6.82
$C_8–C_{19}–H_{20}$	111.0	111.0	111.0	109.4	$O_{17}–C_{11}–O_{18}–C_3$	179.9	179.9	179.9	174.2

cule is rather flexible molecule and, in theory, may have at least four conformers as shown in Fig. 3. Ground state energies, zero point corrected energies (E_{elect} + ZPE), relative energies and dipole moments of conformers were presented in Table 1. Zero point corrections have not caused any significant changes in the stability order.

The optimized molecular geometry (Fig. 3) represents an isolated molecule under ideal conditions with a stationary point at the potential energy surface; the convergence was confirmed by observing no imaginary vibrational wavenumbers. Table 2 shows the selected optimized parameters of 4MESC molecular unit in solid phase using B3LYP (cc-PVDZ, cc-PVTZ and cc-pVQZ) level along with experimental value [39]. The optimized geometry shows that the calculated bond lengths are slightly longer than the experimental values. This variation is due to the fact that the optimization was performed in an isolated condition. The changes in bond length of the C–H bond on substitution are due to the electron donation group within the benzene ring which reduces the electron density of the carbon atom. The agreement for bond angles is not as good as that for the bond distances. The optimized bond lengths of C–C in the ring vary in the range from 1.385 to 1.454 Å for cc-PVDZ level, 1.377 to 1.447 Å for cc-PVTZ and cc-pVQZ levels are in good agreement with 4MESC (1.370–1.445 Å) [39]. The bond length of C–CH_3 (C_8–C_{19}) the calculated value of all the levels are 1.499 and 1.503 Å is also found to deviate negatively only by 0.01 Å in comparison with experimental. C–O bonds in 4MESC vary between 1.359 Å and 1.399 Å and the range of double bonds between C and O are 1.201–1.207 Å [39]. The calculated approximate angles of C_1–C_2–C_3, C_3–C_4–C_5 and C_4–C_8–C_{10} are 119.3°, 118.2° and 118.5°, respectively. The negative deviation of angles and positive deviation of the remaining angles from the normal value of 120° in the ring shows the asymmetry of the benzene ring angles. From the optimized parameters within the coumarin system, the length of the double bond C_4–C_8 1.454 Å, is reasonable for a C=C conjugated to a carbonyl, and the adjacent C_3–C_4 bond of 1.408 Å is shortened because of resonance. In general, the endocyclic and exocyclic C_9–O_{10} bonds in the (hemi) ketals ring show significant deviations from the normal (1.42–1.43 Å). This is explaining the invoking contributions to the ground state from likely resonance structures.

4.2. Natural Bond Orbital Analysis

The natural bond orbital (NBO) analysis provides a description of the structure of a conformer by a set of localized bond, antibonds and Rydberg extra valence orbitals. Stabilizing interactions between filled and unoccupied orbitals and destabilizing interactions between filled orbitals can also be obtained from this analysis [40, 41]. Therefore, NBO theory is a valuable complement to the energetic and structural data presented above. A large number of stabilizing orbital interactions are observed in WS molecule. The NBO [42] analysis is already proved to be an effective tool for chemical interpretation of hyperconjugative interaction and electron density transfer from the filled lone pair electron. The hyperconjugative interaction energy was deduced from the second-order perturbation approach.

$$E(2) = -n_\sigma \frac{\langle \sigma^* | F | \sigma \rangle^2}{\varepsilon_{\sigma^*} - \varepsilon_\sigma} = -n_\sigma \frac{F_{ij}^2}{\Delta E}, \qquad (2)$$

where $\langle \sigma^* | F | \sigma \rangle^2$, or F_{ij}^2 is the Fock matrix element between i and j NBO orbitals, ε_σ and ε_{σ^*} are the energies of σ and σ* NBO's, and n_σ is the population of the donor σ orbital. NBO theory can also be used to identify hydrogen bonding.

Among the most energetic donor-acceptor NBO interactions are those involving the *p*-type lone pair of the oxygen atom, LP2O17 with vicinal σ* (C_{11}–O_{18}) antibonds having energy contribution 222 kJ mol^{-1} of hyperconjugative interaction is weak, these E(2) values and the low value electron density (0.09658e) are chemically significant and can be used as a measure of the intramolecular delocalization. A very strong interaction has been observed between the *p*-type orbital containing the of LP2O13 to the π* (C_5–C_6) and LP2O15 to the π* (C_1–C_2) the neighbor anti-bonding orbital of the benzene ring. This interaction is responsible for a pronounced increases of the O_{13} (1.92095e), O_{15} (1.92022e) orbital occupancy than the other occupancy, and is possible to hyperconjugation between $O_{13, 15}$ and the benzene ring.

The NBO analysis is an efficient method for investigating charge transfer (CT) or hyperconjugative interaction in molecular systems. Some electron donor orbital, acceptor orbital and the interacting stabilization energies resulting from the second-order microdisturbance theory have been reported [43]. The larger the $E^{(2)}$ values are, the more intensive is the interaction between electron donors and electron acceptors. The second-order perturbation theory analysis of Fock matrix in the NBO shows that strong intramolecular hyperconjugative interactions, which are presented in Table 3. The intramolecular hyperconjugative interactions are formed by the orbital overlap between π*(C–C)- and π*(C–C)-bond orbitals which results in intramolecular charge transfer (ICT) causing stabilization of the system. These interactions are observed as an increase in electron density (ED) in C–C antibonding orbital that weakens the respective bonds. The strong intramolecular hyperconjugative interaction of π-electrons from C–C bonds to the π*(C–C)-bond of the phenyl ring increases ED at the six conjugated π-bonds. From the second order perturbation analysis the π-electron

Table 3. Second order perturbation theory analysis of Fock matrix in NBO basis

Donor(i)	ED(i), e	Acceptor(j)	ED(j), e	$E(2)$,[a] kJ mol^{-1}	$E(i)-E(j)$,[b] a.u.	$F(I+j)$,[c] a.u.
$\pi(C_1-C_2)$	1.71559	$\pi^*(C_3-C_4)$	0.40186	191	1339	370
		$\pi^*(C_5-C_6)$	0.31747	123	1392	294
$\pi(C_3-C_4)$	1.65176	$\pi^*(C_1-C_2)$	0.35773	130	1286	291
		$\pi^*(C_5-C_6)$	0.31747	167	1339	339
		$\pi^*(C_8-C_{10})$	0.12235	110	1444	297
$\pi(C_5-C_6)$	1.70372	$\pi^*(C_1-C_2)$	0.35773	182	1313	352
		$\pi^*(C_3-C_4)$	0.40186	135	1313	305
$\pi(C_8-C_{10})$	1.85118	$\pi^*(C_3-C_4)$	0.40186	52	1392	202
		$\sigma^*(C_{11}-O_{17})$	0.21527	161	1497	354
$LP2O_{13}$	1.92095	$\pi^*(C_5-C_6)$	0.31747	138	1785	373
$LP2O_{15}$	1.92022	$\pi^*(C_1-C_2)$	0.35773	141	1812	386
$LP2O_{17}$	1.87352	$\sigma^*(C_{10}-C_{11})$	0.04597	91	3019	381
		$\sigma^*(C_{11}-O_{18})$	0.09658	222	2626	543
$LP2O_{18}$	1.81436	$\pi^*(C_3-C_4)$	0.40186	165	1707	396
		$\sigma^*(C_{11}-O_{17})$	0.21527	205	1838	438

ED – electron density.
[a] $E(2)$ means energy of hyperconjugative interactions; cf. Eq. (2).
[b] Energy difference between donor and acceptor i and j NBO orbitals.
[c] $F(i+j)$ is the Fock matrix element between i and j NBO orbitals.

delocalization around in ph1 and ph2 is revealed by the ED at the three conjugated π-bonds (≈1.65–1.71e) and π*(≈0.31–0.40e) leading to stabilization of 75–95 kJ/mol^{-1}. The π-electron cloud movement from donor to acceptor can make the molecule highly polarized and causes ICT, which is responsible for the NLO activity of 4DMBP.

4.3. HOMO–LUMO Energy

In principle, there are several ways to calculate the excitation energies. The simplest one involves the difference between the highest occupied molecular orbital (HOMO) and the lowest unoccupied molecular orbital (LUMO) of a neutral system, and is a key parameter in determining molecular properties. The eigenvalues of LUMO and HOMO and their energy gap reflect the chemical activity of the molecule. The HOMO energies, the LUMO energies and the energy gap for 4MESC molecules have been calculated using DFT level. An electronic system with a larger HOMO–LUMO gap should be less reactive than one having a smaller gap [44, 45]. The 3D plots of the HOMO and LUMO for the 4MESC are shown in Fig. 4. In 4MESC the highest occupied molecular orbitals are localized mainly on all atoms, the lowest unoccupied molecular orbitals are also mainly on the carbon atoms having single bonds only in the ring, which also indicate that, the frontier molecular orbitals are mainly composed of π-atomic orbitals, so electronic transitions from the HOMO to the LUMO are mainly derived from the electronic transitions of $\pi \rightarrow \pi^*$.

The energy gap between HOMO and LUMO characterizes the molecular chemical stability and their properties and are very important parameters for quantum chemistry. This is also used by the frontier electron density for predicting the most reactive position in π-electron systems and also explains several types of reaction in conjugated system [46]. The conjugated molecules are characterized by a small HOMO–LUMO energy separation, which is the result of a significant degree of intramolecular charge transfer from the end-capping electron–donor groups to the efficient electron–acceptor groups through π-conjugated path [47]. Recently, the energy gap between HOMO and LUMO has been used to prove the bioactivity from intramolecular charge transfer [48, 49]. According to the DFT calculation, the energy gap between (ΔE) transitions from HOMO to LUMO of the molecule is about 4.154 eV. The lower HOMO–LUMO energy gap shows the possibility of intramolecular charge transfer analysis and confirms the bioactivity of the molecule.

4.4. Vibrational Assignments

The molecule 4MESC consists of 22 atoms; hence one can have 60 normal modes of vibrations. The harmonic wavenumber calculations were performed with B3LYP with cc-pVDZ, cc-pVQZ and cc-pVTZ basis sets. The title molecule belongs to C_s point group sym-

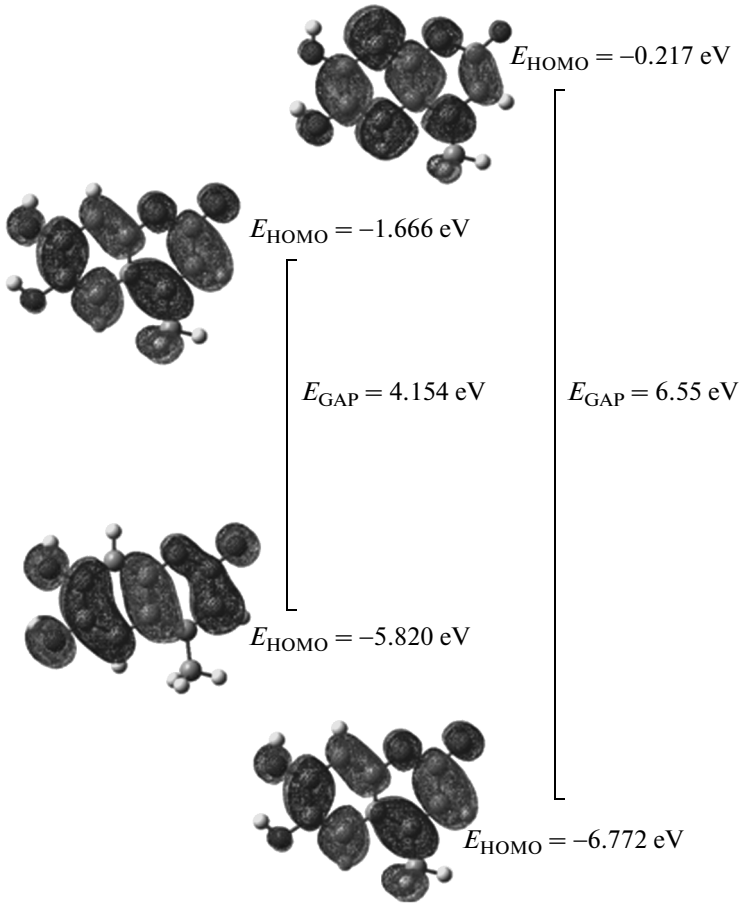

Fig. 4. HOMO–LUMO plot of 4-methylesculetin molecule.

metry. The recorded FT-IR, FT-Raman and calculated wavenumbers and intensities (IR, Raman) are given in Table 4. The comparisons of experimental spectra are shown in Fig. 1 (FT-IR) and Fig. 2 (FT-Raman). The total energy distributions for all fundamental vibrations were calculated using scaled quantum mechanics (SQM) method at B3LYP/cc-pVDZ level.

OH vibrations. The OH group vibrations are likely to be most sensitive to the environment, so they show pronounced shifts in the spectra of the hydrogen-bonded species. The nonhydrogen-bonded or a free hydroxyl group absorbs strongly in the 3700–3550 cm^{-1} region [50, 51]. Theoretically calculated band at 3673 and 3712 cm^{-1} is assigned to the OH symmetric stretching vibration. Experimentally this band is observed in the 3671 and 3707 cm^{-1} region of IR spectra. The O–H in-plane bending vibrations appear in the region 1150–1250 cm^{-1}. While the stretching and out-of-plane of OH group is much affected due to hydrogen bonding, the OH in-plane vibrations are not affected by hydrogen bonded. In-plane OH bending vibration is predicted at 1202 cm^{-1} by cc-pVQZ basis sets (mode no: 38). This vibration is observed experimentally at 1192 cm^{-1} by means of FT-IR spectra. The mode no: 40–41 peaks are mixed bands with OH, ccC, ccH bending vibration and cc, CO stretching vibration.

CH vibrations. Despite six bands expected for the stretching vibrations of the CH group, the FT-IR spectra exhibits only three bands with wavenumbers above 3000 cm^{-1} [52, 53]. According to the performed calculations, the lowest frequency band at 3016 cm^{-1} is definitely due to the asymmetric CH_3 vibration in the FT-IR spectra. Two remaining bands were previously attributed to 3092 cm^{-1} and 3165 cm^{-1} which are assigned to CH stretching vibrations of the ring in the FT-IR spectra.

The in-plane bending vibrations δ(CH) and δ(CH) are observed for 4MESC in the range 890–1180 cm^{-1} (Table 4). Seven modes characterize these vibrations for the δ(CH) ring (ν_{30}, ν_{33}, ν_{34}, ν_{35}, ν_{36}, ν_{37}, and ν_{38}). The IR bands corresponding to these modes are observed at 1022 cm^{-1}, 1119 cm^{-1} and 1159 cm^{-1}. Their Raman peaks are appearing at 891 cm^{-1}, 1092 cm^{-1} and 1164 cm^{-1}.

Table 4. Comparison of the observed and calculated vibrational spectra of free 4MESC molecule

Theoretical (B3LYP)						Experimental		
cc-PVDZ				cc-PVTZ	cc-PVQZ	Exp. IR	Exp. Raman	TED, %
Normal modes	Freq.	I_{IR}	I_{Raman}	Freq.	Freq.			
ν_1	74	0.508	3.916	73	72			$\tau_{CCCH}(15) + \tau_{CCCC}(27) + \tau_{CCCO}(32)$
ν_2	104	0.203	2.759	103	103			$\tau_{CCCC}(36) + \tau_{CCCH}(22) + \tau_{CCCO}(11) + \tau_{CCOC}(18)$
ν_3	168	0.103	6.281	164	163		142	$\tau_{CCCC}(24) + \tau_{CCCO}(15) + \tau_{CCCH}(42)$
ν_4	188	0.405	4.204	187	187		178	$\tau_{CCCC}(30) + \tau_{CCCH}(14) + \tau_{CCCO}(20)$
ν_5	212	0.373	2.810	205	204			$\nu_{CC}(19) + \delta_{CCC}(33) + \delta_{CCO}(23)$
ν_6	213	0.300	2.054	211	212		212	$\tau_{CCCC}(12) + \tau_{CCCH}(70)$
ν_7	266	0.009	6.784	264	264		257	$\tau_{CCOC}(15) + \tau_{CCCC}(23) + \tau_{CCCH}(25) + \tau_{CCCO}(17)$
ν_8	287	25.037	15.686	281	283			$\tau_{CCOH}(71)$
ν_9	294	0.881	3.037	296	297			$\delta_{CCO}(40) + \delta_{CCC}(20)$
ν_{10}	308	0.023	3.856	309	310			$\nu_{CC}(12) + \delta_{CCO}(24) + \delta_{CCH}(11) + \delta_{CCC}(30)$
ν_{11}	369	0.002	28.871	369	371			$\nu_{CC}(10) + \delta_{CCO}(24) + \delta_{CCC}(37)$
ν_{12}	391	2.608	1.874	384	380			$\tau_{CCOH}(17) + \tau_{CCCC}(20) + \tau_{CCCH}(16) + \tau_{CCCO}(28)$
ν_{13}	405	4.646	1.845	399	390		399	$\tau_{CCCH}(10) + \tau_{CCCC}(13) + \tau_{CCOH}(56)$
ν_{14}	409	0.160	38.896	4C10	412			$\nu_{CC}(15) + \delta_{CCO}(23) + \delta_{CCC}(32)$
ν_{15}	448	0.393	6.313	444	445			$\tau_{CCOH}(15) + \tau_{CCCC}(38) + \tau_{CCCH}(19)$
ν_{16}	487	1.759	4.239	487	489	488	473	$\nu_{CC}(16) + \delta_{CCO}(15) + \delta_{CCC}(34) + \delta_{CCH}(15)$
ν_{17}	537	0.854	13.021	538	539	522	529	$\nu_{CC}(11) + \delta_{CCC}(28) + \delta_{CCO}(23)$
ν_{18}	540	0.094	5.755	538	540	545		$\tau_{CCCC}(35) + \tau_{CCCH}(30)$
ν_{19}	560	4.591	5.761	561	565	569	572	$\delta_{CCO}(31) + \delta_{CCC}(25) + \delta_{CCH}(14)$
ν_{20}	646	1.863	13.587	646	649		636	$\nu_{CC}(10) + \delta_{CCO}(27) + \delta_{CCC}(23) + \delta_{CCH}(13)$
ν_{21}	680	0.363	1.464	676	678	663		$\tau_{CCOH}(10) + \tau_{CCCC}(20) + \gamma_{CCH}(24) + \tau_{CCCO}(15)$
ν_{22}	694	0.234	1.169	694	697	691	673	$\tau_{CCOH}(11) + \tau_{CCCC}(42) + \tau_{CCCH}(15)$
ν_{23}	696	1.013	17.902	696	699	710		$\nu_{CC}(20) + \delta_{CCO}(19) + \delta_{CCH}(19)$
ν_{24}	735	0.191	2.127	738	741	741	721	$\tau_{CCOC}(10) + \tau_{CCCC}(28) + \gamma_{CCH}(32) + \tau_{CCCO}(15)$
ν_{25}	776	1.210	12.047	772	775	789	764	$\nu_{CC}(24) + \nu_{CO}(15) + \delta_{CCO}(11) + \delta_{CCC}(25) + \delta_{CCH}(10)$
ν_{26}	817	0.733	1.706	815	818		808	$\nu_{CC}(19) + \nu_{CO}(15) + \delta_{CCC}(22) + \delta_{CCH}(11) + \delta_{CCO}(13)$
ν_{27}	823	3.523	2.540	827	829	839	827	$\tau_{HCCH}(12) + \tau_{CCCC}(13) + \tau_{CCCO}(20) + \gamma_{CCH}(39)$
ν_{28}	850	0.498	1.035	852	855	857	845	$\tau_{CCCC}(14) + \gamma_{CCH}(39) + \tau_{CCCO}(12) + \tau_{OCCH}(19)$
ν_{29}	869	5.618	0.958	869	872		870	$\tau_{CCCC}(28) + \gamma_{CCH}(33) + \tau_{CCCO}(19)$
ν_{30}	893	12.421	15.079	892	897		891	$\nu_{CC}(18) + \nu_{CO}(14) + \delta_{CCO}(11) + \delta_{CCC}(15) + \delta_{CCH}(23)$
ν_{31}	980	1.683	0.875	983	987		960	$\nu_{CC}(11) + \delta_{CCC}(13) + \delta_{CCH}(30) + \tau_{CCCH}(23)$
ν_{32}	1019	0.498	0.132	1028	1032			$\delta_{CCH}(16) + \tau_{CCCC}(21) + \tau_{CCCH}(37)$
ν_{33}	1037	3.350	0.959	1035	1039	1022		$\nu_{CC}(27) + \delta_{CCC}(18) + \delta_{CCH}(21) + \tau_{CCCH}(15)$
ν_{34}	1114	2.536	41.370	1104	1107	1119	1092	$\nu_{CC}(23) + \nu_{CO}(16) + \delta_{CCO}(10) + \delta_{CCH}(23) + \delta_{COH}(11)$
ν_{35}	1136	41.802	25.848	1123	1127			$\nu_{CC}(20) + \nu_{CO}(16) + \delta_{CCC}(11) + \delta_{CCH}(24) + \delta_{COH}(13)$
ν_{36}	1154	2.710	4.382	1149	1153	1159	1164	$\nu_{CC}(16) + \nu_{CO}(15) + \delta_{CCO}(11) + \delta_{CCC}(11) + \delta_{CCH}(27)$
ν_{37}	1182	4.091	18.017	1181	1184			$\nu_{CC}(14) + \delta_{CCC}(11) + \delta_{CCH}(42)$
ν_{38}	1192	4.965	2.760	1196	1202	1196		$\nu_{CC}(14) + \delta_{COH}(19) + \delta_{CCH}(38)$
ν_{39}	1222	2.350	3.334	1222	1227	1245	1244	$\nu_{CC}(15) + \nu_{CO}(10) + \delta_{CCC}(23) + \delta_{CCH}(26)$

Table 4. (Contd.)

Theoretical (B3LYP)						Experimental		
cc-PVDZ				cc-PVTZ	cc-PVQZ	Exp. IR	Exp. Raman	TED, %
Normal modes	Freq.	I_{IR}	I_{Raman}	Freq.	Freq.			
ν_{40}	1270	32.113	5.407	1259	1262	1271		$\nu_{CC}(11) + \nu_{CO}(10) + \delta_{CCC}(26) + \delta_{COH}(13) + \delta_{CCH}(17)$
ν_{41}	1318	6.264	3.642	1300	1303			$\nu_{CC}(26) + \nu_{CO}(11) + \delta_{CCC}(15) + \delta_{CCH}(15) + \delta_{COH}(19)$
ν_{42}	1342	26.132	10.751	1342	1345	1348	1321	$\nu_{CC}(10) + \delta_{CCC}(10) + \delta_{CCH}(16) + \delta_{HCH}(16) + \tau_{CCCH}(24)$
ν_{43}	1362	16.842	8.682	1359	1363		1367	$\nu_{CC}(22) + \delta_{CCC}(10) + \delta_{CCH}(18) + \delta_{HCH}(18)$
ν_{44}	1391	16.403	100	1374	1378	1397	1396	$\nu_{CC}(31) + \delta_{CCC}(16) + \delta_{CCH}(10)$
ν_{45}	1409	1.169	7.285	1432	1438	1437	1431	$\delta_{HCH}(35) + \tau_{CCCH}(52)$
ν_{46}	1418	0.239	6.171	1440	1445			$\delta_{CCH}(15) + \delta_{HCH}(25) + \tau_{CCCH}(35)$
ν_{47}	1461	1.605	9.266	1445	1449	1468	1464	$\nu_{CC}(29) + \delta_{CCC}(16) + \delta_{CCH}(20) + \delta_{CCO}(14)$
ν_{48}	1507	18.819	5.061	1491	1496		1507	$\nu_{CC}(31) + \nu_{CO}(10) + \delta_{CCC}(13) + \delta_{CCH}(24)$
ν_{49}	1576	31.716	62.825	1558	1563	1560	1564	$\nu_{CC}(35) + \delta_{CCC}(14) + \delta_{CCO}(15) + \delta_{CCH}(18)$
ν_{50}	1628	2.801	11.822	1608	1612	1609	1612	$\nu_{CC}(36) + \delta_{CCC}(23) + \delta_{CCH}(19) + \delta_{CCO}(10)$
ν_{51}	1635	10.597	24.551	1612	1617			$\nu_{CC}(30) + \delta_{CCC}(17) + \delta_{CCO}(11) + \delta_{CCH}(22)$
ν_{52}	1774	100	35.082	1741	1741		1746	$\nu_{CC}(20) + \nu_{CO}(26) + \delta_{CCH}(12) + \delta_{CCO}(15)$
ν_{53}	2942	1.686	16.872	2925	2936			$\nu_{CH}(83)$
ν_{54}	3000	1.390	6.788	2970	2982			$\nu_{CH}(75) + \tau_{CCCH}(11)$
ν_{55}	3040	2.194	6.583	3012	3024	3016		$\nu_{CH}(79)$
ν_{56}	3097	0.538	8.016	3071	3083	3092		$\nu_{CH}(75)$
ν_{57}	3114	0.205	10.670	3091	3103			$\nu_{CH}(76)$
ν_{58}	3122	0.322	6.236	3095	3106	3165		$\nu_{CH}(75)$
ν_{59}	3630	18.166	4.811	3650	3673	3671		$\nu_{OH}(92)$
ν_{60}	3676	17.023	7.659	3692	3712	3707		$\nu_{OH}(90)$

Table 5. The NMR spectral data of 4-methylesculetin

	B3LYP (Theoretical)			Experimental		B3LYP (Theoretical)			Experimental
	cc-pVDZ	cc-pVTZ	cc-pVQZ			cc-pVDZ	cc-pVTZ	cc-pVQZ	
C_{11}	145.114	165.389	170.98	161.081	C_{19}	10.644	21.681	24.227	15.663
C_8	143.538	162.016	168.470	151.956	H_9	7.202	7.674	7.861	7.381
C_3	138.492	156.855	162.375	143.077	H_7	6.911	7.244	7.358	7.381
C_1	135.384	153.584	158.969	138.406	H_{12}	6.267	6.543	6.686	6.800
C_6	130.925	148.575	154.128	107.917	H_{14}	5.189	5.942	6.158	6.800
C_4	105.080	120.406	125.623	106.321	H_{16}	4.636	5.336	5.606	5.831
C_{C10}	101.680	115.864	120.783	104.663	H_{20}	2.860	2.997	3.075	2.376
C_5	97.834	113.571	118.811	101.330	H_{21}	2.860	2.997	3.075	2.376
C_2	91.034	105.178	110.385	98.594	H_{22}	2.422	2.664	2.728	2.376

[1]H NMR data taken from [http://www.nmrdb.org/predictor?smiles=C_{12}=CC(=C(O)C=C1C(=CC(O_2)=O)C)O].

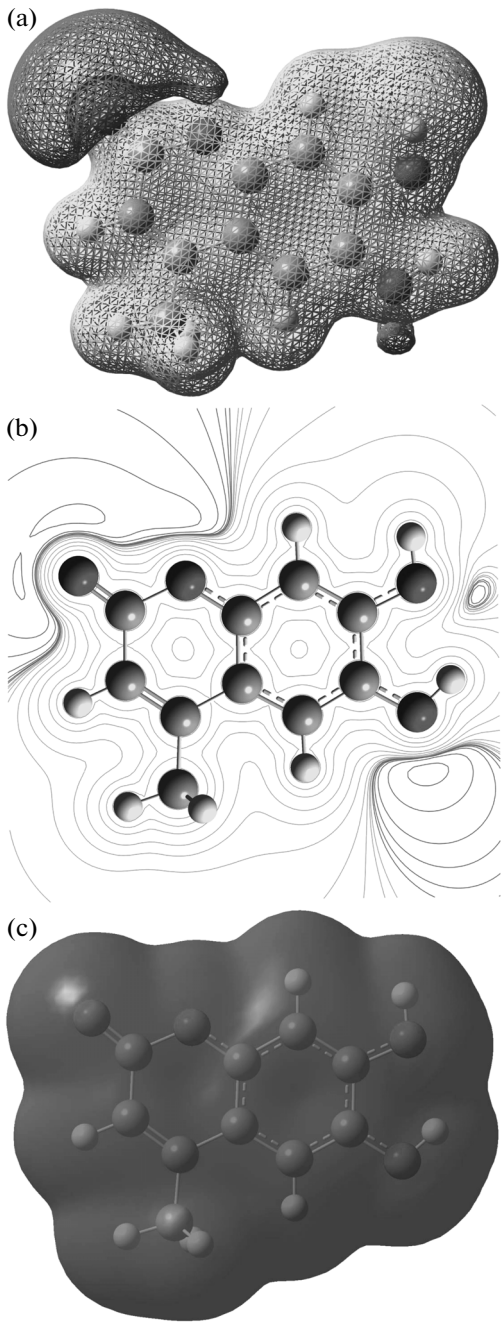

Fig. 5. (a) Molecular electrostatic potential mapped for 4-methylesculetin molecule; (b) molecular electrostatic potential (equipotential lines) mapped for 4-methylesculetin molecule; (c) electron density of e 4-methylesculetin molecule calculated at the B3LYP/cc-pVDZ level of theory.

The out-of-plane CH-bending vibrations appear in the standard region 400–790 cm^{-1}. We predicted at 670–880 cm^{-1} region by B3LYP/cc-pVQZ level of theory. Several bands are observed at 663 cm^{-1}, 741 cm^{-1}, 839 cm^{-1}, and 857 cm^{-1} which are assigned to out-of-plane CH bending vibration of the ring in the FT-IR spectra. These bands observed at 673 cm^{-1}, 721 cm^{-1}, 827 cm^{-1}, 845 cm^{-1}, and 870 cm^{-1} are attributed to out-of-plane bending vibrations of the 4MESC compound in the FT-Raman spectra.

Methyl group vibrations. Vibrations of the C–CH_3 system in 4MESC molecule should be described by 12 normal modes. These are three stretching: 2 ν_{as} (CH_3) and ν_s (CH_3). The CH_3 vibrations of methyl group are predicted at 2936 cm^{-1} (Symmetric), 2982 cm^{-1} (Asymmetric) and 3024 cm^{-1} (Asymmetric) by B3LYP/cc-pVQZ level of theory. Mode numbers are 43 (Symmetric), 45 (Asymmetric) and 46 (Asymmetric) which are assigned to the symmetric CH_3 bending and asymmetric CH_3 bending vibrations of the methyl group. The CH_3 rocking modes are appeared at 987 cm^{-1} (mode no: 31) and 1032 cm^{-1} (mode no: 32) in the 4MESC compound. There is one mode describing torsion mode of the CH_3 group (mode no: 3) these are ν_6 and ν_{10} modes corresponding to the C–CH_3 torsion modes.

4.5. NMR Spectra

Nuclear magnetic resonance (NMR) spectra were recorded to confirm the presence of various types of protons and carbon for the formation of the target compound. The NMR spectra of 4MESC in chloroform solutions were recorded using Bruker Superconducting FT-NMR Spectrometers. All NMR spectra are measured at room temperature. Signals of the recorded NMR spectra are given in Table 5.

The isotropic chemical shifts are frequently used as an aid in identification of reactive ionic species. It is recognized that accurate predictions of molecular geometries are essential for reliable calculations of magnetic properties. The NMR spectra calculations were performed for chloroform solvent. It is necessary to consider the solvent effects because the spectral data available are obtained in different solutions. The isotropic shielding values were used to calculate the isotropic chemical shifts δ with respect to tetramethylsilane (TMS) $\left(\delta_{iso}^{X} = \sigma_{iso}^{TMS} - \sigma_{iso}^{X}\right)$.

4.6. Molecular Electrostatic Potential Maps

The molecular electrostatic potential (MESP) is the most useful electrostatic property to study the relation between structure and activity. The MESP has been also employed as an informative tool of chemistry to describe different physical and chemical features, including non-covalent interactions in complex biological system. The molecular electrostatic potential maps of ESC are shown in Figs. 5a–5c [54].

5. CONCLUSION

FT-IR, FT-Raman and FT-NMR spectra of the 4-methylesculetin molecule have been recorded and analyzed. Density functional theory (DFT) calculations at the B3LYP/cc-pVDZ level has been used to compute energies of different conformers of 4MESC, to find out their stability, the optimized geometry of the most stable conformer and its vibrational spectrum. The observed spectral parameters were seen to be in good agreement with the theoretical data. A complete vibrational analysis has been attempted on the basis of experimental infrared and Raman spectra and calculated frequency and intensity of the vibrational bands and potential energy distribution over the internal coordinates.

ACKNOWLEDGMENTS

Y. Erdogdu would like to thank Ahi Evran University Research Fund for its financial support. Project Numbers: FEN.4003.12.013. Computing resources used in this work were provided by the National Center for High Performance Computing of Turkey (UYBHM).

REFERENCES

1. U. P. Masche, K. M. Rentsch, A. Felten, P. J. Meier, and K. E. Fittinger, Eur. J. Clin. Pharmacol. **54**, 865 (1999).
2. I. Kostova, N. Trendafilova, and G. Momekov, J. Inorg. Biochem. **99**, 477 (2005).
3. G. Luzzatto, F. Fabris, R. D. B. Zanon, and A. Giralami, Arzneim. Forsch. **36**, 972 (1986).
4. I. Kostova, I. Manolov, I. Nicolova, and N. Danchev, Farmaco **56**, 707 (2001).
5. I. Georgieva, I. Kostova, N. Trendafilova, V. K. Rastogi, G. Bauer, and W. Kiefer, J. Raman Spectrosc. **37**, 742 (2006).
6. I. Kostova, N. Trendafilova, and T. Mihailov, Chem. Phys. **314**, 73. (2005).
7. N. Trendafilova, I. Kostova, V. K. Rastogi, I. Georgieva, G. Bauer, and W. Kiefer, J. Raman Spectrosc. **37**, 808 (2006).
8. I. Kostova, N. Trendafilova, and I. Georgieva, Spectrosc. Lett. **40**, 65 (2007).
9. T. Mihaylov, N. Trendafilova, I. Kostova, I. Georgieva, and G. Bauer, Chem. Phys. **327**, 209 (2006).
10. I. Kostova, I. Manolov, I. Nicolova, S. Konstantinov, and M. Karaivanova, Eur. J. Med. Chem. **36**, 339 (2001).
11. I. Kostova, I. Manolov, S. Konstantinov, and M. Karaivanova, Eur. J. Med. Chem. **34**, 63 (1999).
12. I. Manolov, I. Kostova, S. Konstantinov, and M. Karaivanova, Eur. J. Med. Chem. **34**, 853 (1999).
13. Y. Masamoto, H. Ando, Y. Murata, Y. Shimoishi, M. Tada, and K. Takahata, Biosci. Biotechnol. Biochem. **67**, 631 (2003).
14. D. Egan, R. O'Kennedy, E. Moran, D. Cox, E. Prosser, and R. D. Thornes, Derag. Metab. Rev. **22**, 503 (1990).
15. Y. Okata, N. Miyauchi, K. Suzuki, T. Kobayasashi, C. Tsutsui, K. Mayuzumi, S. Nishibe, and T. Okuyama, Chem. Pharm. Bull. **43**, 1385 (1995).
16. M. Paya, B. Halliwell, and J. R. S. Hoult, Biochem. Pharmacol. **44**, 205 (1992).
17. W. L. Lin, C. J. Wang, Y. Y. Tsai, C.L. Liu, J. M. Hwang, and T.H. Tseng, Arch. Toxicol. **74**, 467 (2000).
18. M. Noguchi, M. Arashi, M. Minami, I. Miyazaki, M. Tanaka, and T. Sasaki, Fatty Acids **53**, 325 (1995).
19. A. Palumbo, A. Napolitano, P. Barone, and M. Dischia, Chem. Res. Toxicol. **12**, 1213 (1999).
20. M. L. Bretikbe, C. Servy, M. Lenfant, and C. Ducrocq, Tetrahedron Lett. **35**, 7231 (1994).
21. J. P. Abraham, I. H. Joe, V. George, O. F. Nielsen, and V. S. Jayakumar, Spectrochim. Acta A **59**, 193 (2003).
22. D. Sajan, I. H. Joe, J. Zaleski, and V. S. Jayakumar, Laser Phys. Lett. **2**, 343 (2005).
23. R. G. Parr and W. Yang, *Density Functional Theory of Atoms and Molecules* (Oxford, New York, 1989).
24. (a) R. O. Jones and O. Gunnarson, Rev. Mol. Phys. **61**, 689 (1989); (b) T. Ziegler, Chem. Rev. **91**, 651 (1991).
25. W. Kohn and L. J. Sham, Phys. Rev. A **140**, 1133 (1965).
26. C. James, G. R. Pettit, O. F. Nielsen, V. S. Jayakumar, and I. H. Joe,Spectrochim. Acta A **70**, 1208 (2008).
27. A. D. Becke, J. Chem. Phys. **98**, 5648 (1993).
28. C. Lee, W. Yang, and R. G. Parr, Phys. Rev. B **37**, 785 (1988).
29. M. J. Frisch, G. W. Trucks, H. B. Schlegel, G. E. Scuseria, M. A. Robb, J. R. Cheeseman, J. A. Montgomery, Jr., T. Vreven, K. N. Kudin, J. C. Burant, J. M. Millam, S. S. Iyengar, J. Tomasi, V. Barone, B. Mennucci, M. Cossi, G. Scalmani, N. Rega, G. A. Petersson, H. Nakatsuji, M. Hada, M. Ehara, K. Toyota, R. Fukuda, J. Hasegawa, M. Ishida, T. Nakajima, Y. Honda, O. Kitao, H. Nakai, M. Klene, X. Li, J. E. Knox, H. P. Hratchian, J. B. Cross, C. Adamo, J. Jaramillo, R. Gomperts, R. E. Stratmann, O. Yazyev, A. J. Austin, R. Cammi, C. Pomelli, J. W. Ochterski, P. Y. Ayala, K. Morokuma, G. A. Voth, P. Salvador, J. J. Dannenberg, V. G. Zakrzewski, S. Dapprich, A. D. Daniels, M. C. Strain, O. Farkas, D. K. Malick, A. D. Rabuck, K. Raghavachari, J. B. Foresman, J. V. Ortiz, Q. Cui, G. Baboul, S. Clifford, J. Cioslowski, B. B. Stefanov, G. Liu, A. Liashenko, P. Piskorz, Komaromi, R. L. Martin, D. J. Fox, T. Keith, M. A. Al-Laham, C. Y. Peng, A. Nanayakkara, M. Challacombe, P. M. W. Gill, B. Johnson, W. Chen, M. W. Wong, C. Gonzalez, and J. A. Pople, Gaussian 03, Revision C.02 (Gaussian, Inc., Wallingford, 2004).
30. H. B. Schlegel, J. Comput. Chem. **3**, 214 (1982).
31. Spartan 10, Wavefunction Inc., Irvine, CA 92612, USA (2010).
32. G. Rauhut and P. Pulay, J. Phys. Chem. **99**, 3093 (1995).
33. D. Michalska, Raint Program (Wroclaw Univ. Technol., 2003).
34. D. Michalska and R. Wysokinski, Chem. Phys. Lett. **403**, 211 (2005).

35. R. Ditchfield, Molecular Orbital Theory of Magnetic Shielding and Magnetic Susceptibility **56**, 5688 (1972).
36. K. Wolinski, J. F. Hinton, and P. Pulay, J. Am. Chem. Soc. **112** (23), 8251 (1990).
37. N. Azizi, A. A. Rostami, and A. Godarzian, J. Phys. Soc. Jpn. **74**, 1609 (2005).
38. M. Rohlfing, C. Leland, C. Allen, and R. Ditchfield, Chem. Phys. **879**, 15 (1984).
39. S. P. Yang, L. J. Han, D. Q. Wang, and H.T. Xia, Acta Cryst. E **63**, 4785 (2007).
40. A .E. Reed, L.A. Curtiss, and F. Weinhold, Chem. Rev. **88**, 899 (1988).
41. J. P. Foster and F. Weinhold, J. Am. Chem. Soc. **102**, 7211 (1980).
42. E. D. Glendening, A. E. Reed, J. E. Carpenter, and F. Weinhold, NBO Version 3.1, TCI, University of Wisconsin, Madison, 1998.
43. C. James, A. Amal Raj, O. F. Nielson, V. S. Jayakumar, and I. Hubert Joe, Spectrochim. Acta A **70**, 1208 (2008).
44. R. Kurtaran, S. Odabas, O. Glu, Azizoglu, H. Kara, and O. Atakol, Polyhedron **26**, 5069 (2007).
45. D. A. Dixon and B. E. Smart, Chem. Eng. Commun. **98**, 173 (1990).
46. K. Fukui, T. Yonezawa, and H. Shingu, J. Phys. Chem. **20**, 722 (1952).
47. C. H. Choi and M. Kertesz, J. Phys. Chem. A **101**, 3823 (1997).
48. D. Sajan, R. Reshmy, K. Kurien Thomas, Y. Erdogdu, and I. Hubert Joe, Spectrochim. Acta A **99**, 234 (2012).
49. C. Ravikumar, I. H. Joe, and V. S. Jayakumar, Chem. Phys. Lett. **460**, 552 (2008).
50. Y. Erdogdu, O. Ünsalan, and M. T. Güllüoğlu, J. Raman Spectrosc. **41** (7), 820 (2010).
51. D. Sajan, Y. Erdogdu, R. Reshmy, Ö. Dereli, K. K. Thomas, and I. Hubert Joe, Spectrochim. Acta A **82**, 118 (2011).
52. O. Ünsalan, Y. Erdogdu, and M. T. Güllüoğlu, J. Raman Spectrosc. **40** (5), 562 (2009).
53. M. T. Güllüoğlu, Y. Erdogdu, J. Karpagam, N. Sundaraganesan, and Ş. Yurdakul, J. Mol. Struct. **99**, 14 (2011).
54. Y. Erdogdu, Spectrochim. Acta A **106**, 25 (2013).